Ⅳ. 研究成果の刊行物・別冊

Permeation Pathway of Macromolecules and Nanospheres through Skin

Hiroaki TODO,[a] Eriko KIMURA,[a] Hirotaka YASUNO,[a] Yoshihiro TOKUDOME,[a] Fumie HASHIMOTO,[a] Yoshiaki IKARASHI,[b] and Kenji SUGIBAYASHI*[,a,c]

[a] *Faculty of Pharmaceutical Sciences, Josai University;* [c] *Life Science Research Centre, Josai University; 1–1 Keyakidai, Sakado, Saitama 350–0295, Japan; and* [b] *National Institute of Health Sciences; 1–18–1 Kamiyoga, Setagaya-ku, Tokyo 158–8501, Japan.* Received February 15, 2010; accepted May 31, 2010; published online June 1, 2010

The permeation pathway of macromolecules and nanospheres through skin was evaluated using fluorescent isothiocyanate (FITC)-dextran (average MW, 4 kDa) (FD-4) and nanospheres (500 nm in diameter) in hairless rat abdominal skin and porcine ear skin as well as a three-dimensional cultured human skin model (cultured skin model). A low molecular hydrophilic compound, sodium fluorescein (FL) (MW, 376 Da), was used for comparison. FL penetrated the stratum corneum and permeated the viable epidermis of hairless rat skin, whereas less permeation of FL was observed through the cultured skin model, suggesting that the primary permeation pathway for the hydrophilic material may be skin appendages through the rat skin. A macromolecular compound, FD-4, was distributed through the hair follicles of the rat skin. In addition, nanospheres were detected in the hair follicles of porcine skin, although no skin permeation was detected. These findings suggest that appendage routes such as hair follicles can be a penetration pathway of macromolecules and nanospheres through skin.

Key words macromolecule; nanosphere; skin permeation pathway; transdermal drug delivery; hair follicle

Delivery of macromolecular compounds and nano-/microparticles has become more realistic due to the recent development of new tools and nanotechnologies for delivery enhancement.[1,2] The administration sites of such macromolecules and nano-/microparticles are supposed to be the mucosa, such as the gastrointestinal (GI) tract,[3] and ophthalmic, nasal and pulmonary[4] mucosa and skin.[5,6] Skin has been paid particular attention as an attractive administration site of these compounds because of its accessibility and easy application. Emulsion droplets, liposomes and other lipophilic carriers[7] containing small molecular active ingredients have already been investigated in the cosmetic field as well as therapeutic drug areas; however, the stratum corneum, the outermost layer of skin, has a primary function to protect the invasion and skin penetration of exogenous substances. Generally, only small molecular compounds less than 500 Da molecular weight are capable of significant passive permeation through the skin barrier (known as the 500 Dalton rule).[8] Thus, skin permeation of macromolecular compounds or nano-/microparticles is very difficult or impossible. Many reports have suggested that large molecules are likely to accumulate on the skin surface or appendages such as hair follicles.[9–12] Nevertheless, few reports have shown a quantitative approach for hair follicular penetration using quantitative skin permeation parameters.

Hairless rat and pig ear skins and three-dimensional cultured human skin model would be useful skin models with and without hair follicles, respectively, to clarify the contribution of hair follicles to skin permeation or the distribution of macromolecules and nanospheres.

In the present study, we selected fluorescent isothiocyanate (FITC)-dextran (average MW, 4 kDa) (FD-4) as a model macromolecular weight compound and 500 nm fluorescent polystyrene latex spheres as model nanospheres, and their potential for skin delivery was investigated by calculating skin permeation parameters or measuring the skin distribution of FD-4 and fluorescent polystyrene latex nanospheres in hairless rat abdominal skin and porcine ear skin as well as a three-dimensional cultured human skin model. Tables 1 and 2 summarize the model penetrant compounds and skin membranes used in this experiment. A low molecular hydrophilic compound, sodium fluorescein (FL) (MW 376 Da), was also used for comparison.

Theoretical Skin permeation kinetics is usually evaluated under an assumption that the skin consists of a single barrier membrane against drug permeation; however, generally, the drug-permeable membrane must be classed into three membranes: dissolution–diffusion membrane (Type 1 membrane), porous membrane (Type 2 membrane) and composite membrane (Type 3 membrane) of Type 1 and 2 membranes. Under the assumption that a single barrier of skin is one of these three membranes, the steady state skin permeation rate per unit application area, dQ/dt, is expressed using Fick's first law of diffusion as follows:

Type 1 membrane (dissolution–diffusion membrane)

$$\frac{dQ}{dt} = D \cdot \frac{K \cdot C_v}{L} = (KL)\left(\frac{D}{L^2}\right)C_v \tag{1}$$

Type 2 membrane (porous membrane)

$$\frac{dQ}{dt} = \frac{\varepsilon \cdot D_p}{\tau} \cdot \frac{C_v}{L} = (\varepsilon L)\left(\frac{D_p}{\tau L^2}\right)C_v \tag{2}$$

Type 3 membrane (composite membrane)

$$\frac{dQ}{dt} = (1-\varepsilon) \cdot D \cdot \frac{K \cdot C_v}{L} + \frac{\varepsilon \cdot D_p}{\tau} \cdot \frac{C_v}{L} = \left[\{(1-\varepsilon)KL\}\left(\frac{D}{L^2}\right) + (\varepsilon L)\left(\frac{D_p}{\tau L^2}\right)\right]C_v \tag{3}$$

where C_v is the initial concentration of the applied compound, D, K and L are diffusion coefficient, partition coefficient and barrier thickness of the membrane, respectively, and D_p, ε and τ are diffusion coefficients in water-filled pores, average fraction of diffusion area of pores, and tortuosity of the membrane, respectively. In examples 1 and 2, partition parameters and diffusion parameters of the pene-

* To whom correspondence should be addressed. e-mail: sugib@josai.ac.jp

trant are KL and DL^{-2} for the Type 1 membrane and εL and $D_p\tau^{-1}L^{-2}$ for the Type 2 membrane, respectively. The permeability coefficient, P, can be obtained as a product of the partition parameter and diffusion parameter. Diffusion lag time was obtained by dividing six by the diffusion parameter.

MATERIALS AND METHODS

Materials and Animals Both FL and FD-4 were obtained from Sigma-Aldrich Co., Ltd. (St. Louis, MO, U.S.A.). Fluorescent polystyrene latex nanospheres, Fluoresbrite® yellow green carboxylate microspheres (500 nm in average diameter), were purchased as model nanospheres from Polysciences, Inc. (Warrington, PA, U.S.A.). All other reagents and solvents were of reagent grade or HPLC grade, and used without further purification.

Male hairless rats (WBN/ILA-Ht, *ca.* 200—250 g) were supplied either from Life Science Research Center, Josai University (Sakado, Saitama, Japan) or Ishikawa Experimental Animal Laboratory (Fukaya, Saitama, Japan). Porcine ear skins were from Saitama Experimental Animal Laboratory (Sugito, Saitama, Japan). A three-dimensional cultured human skin model, Living Skin Equivalent-high (LSE-high), was obtained from Toyobo (Osaka, Japan).

Determination of *n*-Octanol–Water Partition Coefficient *n*-Octanol–water partition coefficient ($K_{o/w}$) of each fluorescent compound (FL or FD-4) was measured using distilled water–saturated *n*-octanol and *n*-octanol–saturated pH 7.4 phosphate buffered saline (PBS) at 32 °C. *n*-Octanol was added to the same volume of pH 7.4 PBS containing 10 mg/ml of each fluorescent, and the thoroughly mixed solution was equilibrated for 24 h. The aqueous phase was then analyzed using a fluorescence spectrophotometer (RF 5300PC; Shimadzu, Kyoto, Japan) at excitation and emission wavelengths of 490 and 520 nm, respectively. Logarithmic values of the partition coefficients are shown in Table 1.

***In Vitro* Skin Permeation Study** The skin permeation of FL and FD-4 was assessed using excised hairless rat abdominal skin and LSE-high. After the rats had been anesthetized by intraperitoneal injection of sodium pentobarbital (50 mg/kg), the abdominal skin was excised as described in our previous paper.[14] Stripped hairless rat skin was also used after removing the stratum corneum from the abdominal area by stripping 20 times with adhesive tape (Cellophane tape; Nichiban Co., Ltd., Tokyo, Japan). LSE-high was used after removing cultured skin pieces from the plastic insert with a knife. Each skin membrane was mounted in the side-by-side diffusion cell (effective diffusion area: 0.95 cm^2),[15,16] and 1.0 mM FL or 0.25 mM FD-4 (2.5 ml each) was applied to the stratum corneum side and the same volume of PBS was applied to the dermal side. Samples of 0.40 ml were taken periodically from the dermal side compartment, and then the same volume of the same solvent was added to keep the volume constant. FL or FD-4 concentration of each sample was determined using a fluorescence spectrophotometer, as explained above. The hairless rat skin and LSE-high surfaces were carefully rinsed with PBS several times to remove FL or FD-4 attached to the stratum corneum 6 h after starting the experiment. The obtained skin sample was embedded in Tissue-Tek® OTC compound (Miles, Inc., Elkhart, IN, U.S.A.) and stored at −80 °C until slicing.

Table 1. Physicochemical Properties of Model Compounds

Model compounds (abbreviation)	Molecular weight (Da)	Mean particle size or molecular radius	Log $K_{o/w}$ [a]
Sodium fluorescein (FL)	376	0.45 nm[13] (Stokes radius)	−0.615
FITC-dextran (FD-4)	4000	1.4 nm (Stokes radius)[13]	−0.773
Fluorescent polystyrene latex nanospheres (Fluoresbrite)	—	500 nm	—

a) $K_{o/w}$: *n*-octanol–water partition coefficient.

The skin permeation property of fluorescent polystyrene latex spheres (Fluoresbrite) was evaluated using excised hairless rat skin and excised porcine ear skin, which had been carefully shaved and the underlying excess fatty tissues removed from the dermis. LSE-high was also used to evaluate whether Fluoresbrite permeates the cultured skin. The obtained skin membranes were mounted in a Franz-type diffusion cell[14] (effective diffusion area: 1.77 cm^2). Then, 1.0 ml PBS-suspended solution containing Fluoresbrite (3.64×10^{10} particles/ml for 500 nm spheres) was applied to the stratum corneum surface, whereas 6.0 ml PBS was applied to the dermal side. The skin permeation test was performed at 32 °C over 12 h through hairless rat skin, porcine ear skin and LSE-high, while the receiver solution was continuously stirred with a star-head-type magnetic stirrer. The receiver solution was withdrawn 12 h after beginning the permeation experiment. The skins were then carefully rinsed with PBS several times to remove polystyrene spheres attached to the stratum corneum 12 h after starting the experiment. The obtained skin sample was embedded in Tissue-Tek® OTC compound (Miles, Inc., Elkhart, IN, U.S.A.) and stored at −80 °C until slicing.

All animal experiments were approved by the Institutional Animal Care and Use Committee of Josai University.

Evaluation of Skin Permeation Kinetics Steady-state flux was calculated by linear regression of the linear portion of normalized cumulative amount of penetrant permeated *versus* the time-curve (steady state; reached 4—6 h after starting the experiment), and the lag time was calculated from the intercept on the time axis by extrapolation from the steady state skin permeation profile. The normalized cumulative amount of penetrant permeated, Q_n, was calculated by dividing the cumulative amount permeated per unit area of skin by the initial concentration of the applied fluorescent compound in the donor compartment.[17] The permeation parameters were obtained by curve fitting the skin permeation data by Scheuplein's equation,[18] which comes from Fick's second law of diffusion. The least squares curve fitting method was performed using Microsoft® Excel Solver.[19] The calculation condition was 100 s for the calculation limit, 100 times for repeated calculation, 10^{-6} for accuracy, 5% basic tolerance and 10^{-3} for convergence. The pseudo-Newtonian method was used as an algorithm.

Sectioning of Hairless Rat Skin, Porcine Ear Skin and LSE-High Hairless rat skin, porcine ear skin and LSE-high embedded in Tissue-Tek® OTC compound were sequentially sliced with a cryostat (CM3050S; Leica, Wetzlar, Germany) to obtain horizontal and vertical 20 μm-thick sections. The prepared skin sections were observed with a fluorescence mi-

Table 2. Comparison of Skin Thickness and Presence or Absence of Hair Follicles in Several Skin Models

Skin model	Skin structure constitution	Stratum corneum thickness (μm)	Epidermis thickness (μm)	Whole skin thickness (mm)	Skin appendage	Relationship to human skin permeation
Hairless rat skin	Epidermis/dermis	15.4 ± 3.3[20]	23.8 ± 5.3[20]	0.86 ± 0.06[20]	Yes	High
Pig skin	Epidermis/dermis	10.6 ± 0.5	52.5 ± 4.1	1.2 ± 0.002	Yes	High
LSE-high	Epidermis/dermis	27.0 ± 0.7	31.4 ± 1.3	0.12 ± 0.001	No	High

croscope (CK40; Olympus Corp., Tokyo, Japan).

Measurement of Thickness in LSE-High and Porcine Skin The thicknesses of the stratum corneum, epidermis, and whole skin in LSE-high and porcine skin were microscopically determined from microtomed sections after hematoxylin–eosin staining. Five good sections from each specimen were used to measure the stratum corneum, and whole skin thicknesses were measured by a light micrograph (IX71; Olympus Corp., Tokyo, Japan) and a calibrated ocular micrometer. The thickness of the epidermis was calculated by subtracting the stratum corneum thickness from the whole skin thickness. The thickness of hairless rat skin was cited from our previous paper.[20]

Observation of Skin Surface Shaved hairless rat and porcine ear skins were mounted with adhesive tape on a scanning microscopy (SEM) stage, and the skin surface was observed without coating by a low-vacuum SEM (S-3000N; Hitachi Ltd., Tokyo, Japan).

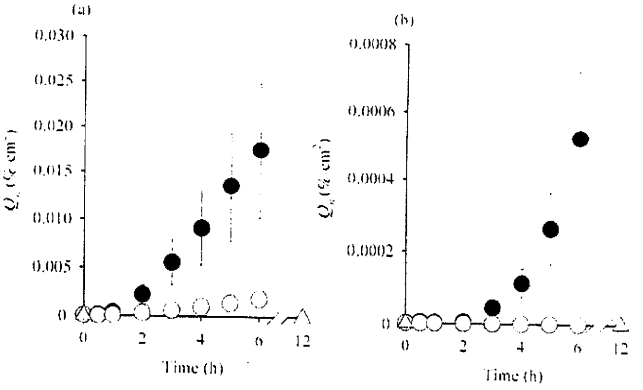

Fig. 1. Cumulative Amount of Hydrophilic Fluorescent Compounds, FL (●), FD-4 (○) and 500 nm Fluoresbrite (△) through Hairless Rat Skin (a) and LSE-High (b)

Normalized cumulative amount of the compounds permeating a percent per unit application area (%/cm^2)[17] was plotted on the vertical axis. Each data point represents the mean±S.E. of 3—4 experiments.

RESULTS

Many reports have shown that nano-/microspheres could not permeate the healthy stratum corneum.[21] In our study, therefore, the penetration pathway of hydrophilic fluorescent markers, FL and FD-4, was observed to evaluate the potential penetration of these mal-absorptive materials into skin and the delivery pathway through the skin barrier. The characteristics of model skin membranes (excised hairless rat skin, pig ear skin and LSE-high) are shown in Table 2. The stratum corneum in LSE-high was much thicker than the others. In addition, skin appendages such as sweat ducts and hair follicles could not be observed in LSE-high. Although many structural differences could be found between LSE-high and the others, and the permeation of several compounds (MW 122—236, $-1.5 < \log K_{o/w} < 2.1$) through LSE-high was about 10 times higher than through hairless rat and human skins, and the permeation rate through LSE-high showed a linear relationship to that through hairless rat and human skins.[14]

Figure 1a and b show the time course of the normalized cumulative amount of FL and FD-4 that permeated the unit area of excised hairless rat skin and LSE-high, respectively. In these experiments, 1.0 mM FL or 0.25 mM FD-4 (2.5 ml each) was applied to the skin surface to follow skin permeation. Interestingly, both fluorescent markers permeated hairless rat skin, whereas less permeation of FL and no permeation of FD-4 were observed through LSE-high. The Q_n of FL through hairless rat skin was 30-fold higher than through LSE-high.

The typical lag time and subsequent steady state permeation were observed for the permeation of both fluorescents through hairless rat skin. Permeability coefficients of FL and FD-4 were calculated by two methods using steady-state flux (observed value) and the curve fitting method (estimated value). These values are summarized in Table 3. The estimated vales were almost equal to the corresponding observed values and no significant differences appeared in hairless rat data. The calculated values of the permeability coefficient and Q_n of FL through LSE-high were about one-twelfth and one-thirtieth through hairless rat skin, respectively; furthermore, the lag time of FL through LSE-high (estimated value) was about three-fold of that through hairless rat skin. On the other hand, lag times of FL and FD-4 through hairless rat skin were almost the same as those through LSE-high.

Fluoresbrite was also applied to hairless rat skin and LSE-high. Although a Franz-type diffusion cell was used for measuring the skin permeation of Fluoresbrite, no permeation of the nanospheres was detected 12 h after starting the skin permeation experiment (see Fig. 1). No skin permeation was detected when Fluoresbrite was applied to porcine ear skin (data not shown).

Figure 2 shows fluorescent photographs illustrating the skin distribution of FL and FD-4 in hairless rat skin and LSE-high after topical application of these fluorescent markers. High-intensity FL was detected both in the stratum corneum and hair follicles of hairless rat (Fig. 2a), whereas FD-4 was mainly observed in the hair follicles (Fig. 2b). On the other hand, with LSE-high, FL was detected mostly in the stratum corneum and slightly in the viable epidermis (Fig. 2c) and FD-4 was found only on the skin surface (no skin penetration was observed for FD-4) (Fig. 2d). These results also suggest the high contribution of the transfollicular pathway to the transport of mal-absorptive hydrophilic compounds across the skin. In addition, this tendency was more

Table 3. Lag Time and Permeability Coefficients of FL and FD-4 through Excised Hairless Rat Skin or LSE-High

		FL		FD-4	
		Lag time (h)	Permeability coefficient (cm/s)	Lag time (h)	Permeability coefficient (cm/s)
Hairless rat	Estimated value[a]	2.0±0.16	$(1.1\pm0.5)\times10^{-8}$	2.2±0.01	$(3.6\pm0.2)\times10^{-9}$
	Observed value[b]	1.8±0.20	$(1.2\pm0.5)\times10^{-8}$	2.1±0.01	$(3.4\pm0.2)\times10^{-9}$
LSE-high	Estimated value[a]	5.4±0.4	$(9.4\pm2.4)\times10^{-10}$	—	$\ll1.21\times10^{-10}$
	Observed value[b]	—[c]	—[c]	—[c]	—[c]

a) Estimated value was calculated by curve-fitting the time course of the cumulative amount of skin permeation of compounds using Scheuplein's equation.[25] *b*) Observed value was obtained by the slope of steady-state flux and time-axis intercept of the time course of the cumulative amount of skin permeation of compounds. *c*) No steady state permeation was obtained until 6 h in the skin permeation study. *d*) Estimated value was calculated from lower quantitative limit of FD-4 in receiver cell 6 h after skin permeation study.

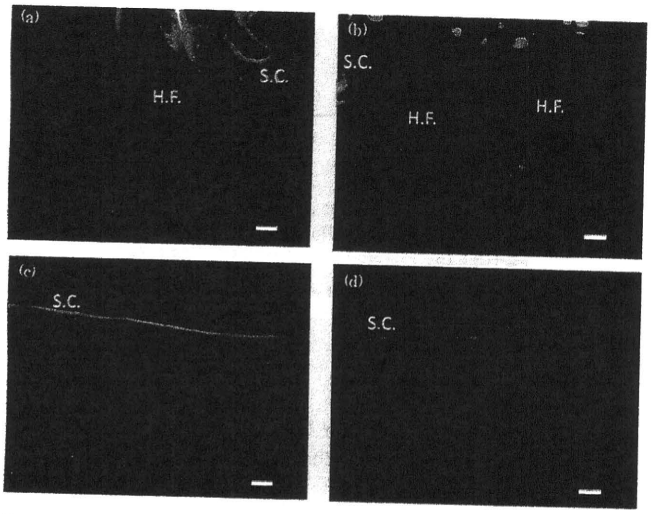

Fig. 2. Histological Observation of Hairless Rat Intact Skin (a, b) and LSE-High (c, d) after Application of FL (a, c) and FD-4 (b, d)

S.C.: Stratum corneum; H.F.: hair follicle. White bars=100 μm. (a, b): Fluorescence derived from FL or FD-4 was observed on the skin surface of skin and in hair follicles. (c, d): fluorescence derived from FL or FD-4 was observed in shallow areas or only on the surface, respectively, of LSE-high.

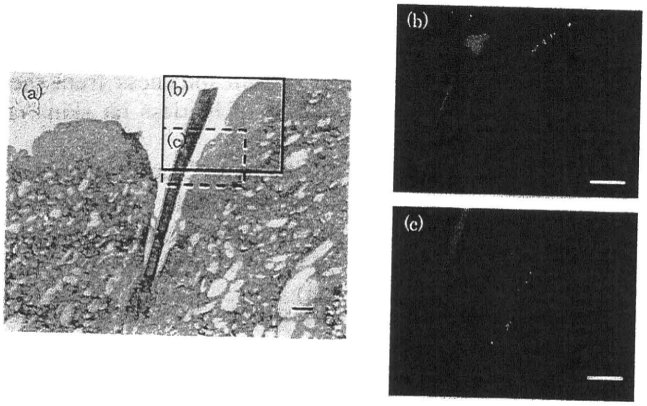

Fig. 3. Histological Observation of Excised Porcine Ear Skin 12 h after Application of 500 nm Fluoresbrite

a: Light micrograph of vertical slice. b and c: Fluorescent micrograph of area b and c in Fig. 3a. Bar=200 μm. (b, c): Fluoresbrite was observed in infundibulum of the hair follicle and surface of the hair shaft.

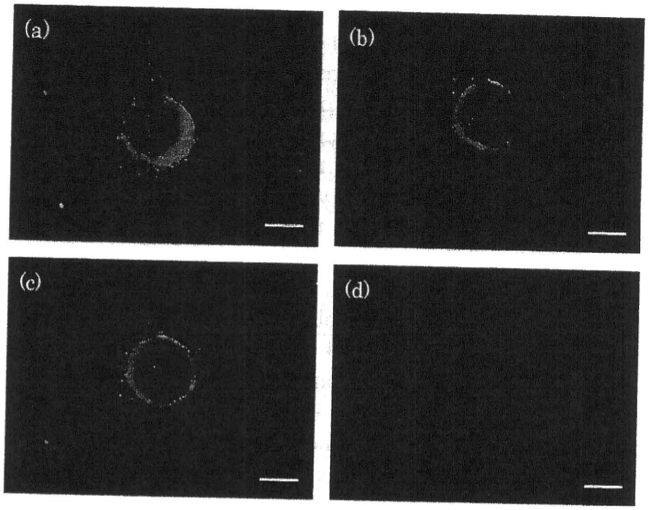

Fig. 4. Localization of 500 nm Fluoresbrite Penetrating the Hair Follicle

Fluorescence images (a—d) are horizontal slices at different depths from the skin surface of excised porcine ear skin 12 h after application of particles. a: *ca.* 20 μm, b: 40—60 μm, c: 80—100 μm, d: 200—220 μm. Bar=100 μm. (a): Fluoresbrite was detected on the surface of hair shaft and connective tissue in the follicle. (b, c): number of particles gradually decreased with an increase in depth from the skin surface. (d) only autofluorescence was observed.

marked when using the macromolecular compound. Thus, skin appendages such as hair follicles must be very important for the skin permeation of malabsorptive compounds.

Next, the skin distribution of Fluoresbrite (500 nm in diameter) was investigated after topical application to excised hairless rat skin, excised porcine ear skin and LSE-high. Nanospheres were detected only on the surface of the stratum corneum (data not shown) for hairless rat skin and LSE-high; therefore, a detailed observation was performed using excised porcine skin, since it has much larger hair follicles. Figure 3a shows a light microphotograph of porcine skin (vertical slice of hair follicle area) 12 h after the application of Fluoresbrite, and Figure 3b and c show fluorescent microphotographs of specific parts of the hair follicle area, as explained in Fig. 3a. Many nanospheres were found around the openings of the hair follicle, especially close to the epidermis side and around the hair shaft, as shown in Fig. 3b and c. The penetration depth of Fluoresbrite in the hair follicles was investigated by preparing horizontal slices of the hair follicle area of skin. The thickness of each skin section was adjusted to 20 μm. Figure 4 shows typical cross-section images of the hair follicle area from the skin surface (0—20 μm) to dermis side (200—220 μm) 12 h after application of Fluoresbrite to the excised porcine ear skin. In accordance with the photograph in Fig. 3, nanospheres could be detected in hair follicles, such as the surface of the hair shaft and connective tissue follicles, and the intensity due to nanospheres in the hair follicle gradually decreased with increasing pene-

tration depth; however, nanospheres could not be detected in connective tissue follicles below 200-μm depth from the skin surface. Only greenish-yellow autofluorescence derived from keratin and melanin was observed in Fig. 4d. This result clearly identified that the nanospheres were distributed or penetrated until about 100-μm depth, but did not penetrate as far as 200-μm depth from the skin surface 12 h after application. Thus, macromolecular compounds, such as FD-4 and nanospheres, are probably distributed or penetrate through the transfollicular pathway, although the extent is very marginal.

DISCUSSION

Three kinds of membranes are frequently utilized to describe the membrane permeation profiles of compounds, as explained in the theoretical section. In the dissolution–diffusion membrane (Type 1 membrane), compounds are dissolved and distributed into the membrane and then diffused in the homogeneous membrane. In the microporous membrane (Type 2 membrane), compounds are diffused across solvent (usually aqueous)-filled pores in the membrane. The third membrane (composite membrane) is the previous two membranes combined.

In the case of hairless rat and porcine skins, the stratum corneum and skin appendage may be the permeation pathway of compounds, especially for low molecular compounds ($\leq$500 Da). Thus, these animal skins would be assumed to be the third membrane. On the other hand, LSE-high would be classified as a dissolution–diffusion membrane, since three-dimensional cultured human skin model has no appendages, such as hair follicles and sweat ducts.

Although LSE-high is such a skin appendage-deficiency model, it was observed in our previous study[14] that logarithmic values of the permeability coefficient, $\log P$, of seven drugs through LSE-high were fairly proportional to those through excised hairless rat, pig and human skins, and the partition parameters of LSE-high were almost the same as in other skins. For FL and FD-4 applied to LSE-high, low permeation and no permeation were observed in the present study, while permeation through hairless rat skin was observed. The permeability coefficient, P, of FD-4 through LSE-high was calculated from the lower quantitative limit of FD-4 in receiver solution (Table 3). The estimated value was about thirtieth of that of FD-4 through hairless rats. FL (pK_a 1: 4.32, pK_a 2: 6.5)[22] predominantly exists as an ionized form in pH 7.4 PBS, and FD-4 has a high molecular weight; therefore, the P-value of FL and FD-4 through LSE-high was much lower than through hairless rat skin.

The P-value is a product of the partition parameter (KL or εL) and diffusion parameter (DL^{-2} or $D_p\tau^{-1}L^{-2}$).[23] To clarify the differences of skin permeation profiles between hairless rat skin and LSE-high, the partition parameter and diffusion parameter were compared.

Table 4 shows the partition and diffusion parameters, which were calculated from curve-fitting the time course of the cumulative amount of FL and FD-4 permeating hairless rat skin and LSE-high. Interestingly, both parameters of LSE-high calculated from FL permeation were not the same as those of hairless rat skin. These differences might reflect the different permeation routes of FL between these skins.

Table 4. Comparison of Partition Parameter and Diffusion Parameter between Hairless Rat Skin and LSE-High

Compound	Membrane	Partition parameter (KL or εL) (cm)	Diffusion parameter (DL^{-2} or $D_p\tau^{-1}L^{-2}$) (s^{-1})
FL	Hairless rat	$(4.7\pm1.8)\times10^{-4}$	$(2.3\pm0.18)\times10^{-5}$
	LSE-high	$(1.1\pm0.31)\times10^{-4}$	$(8.6\pm0.75)\times10^{-6}$
FD-4	Hairless rat	$(1.7\pm0.13)\times10^{-4}$	$(2.0\pm0.06)\times10^{-5}$
	LSE-high	—	—

KL and DL^{-2} or εL and $D_p\tau^{-1}L^{-2}$ were calculated by curve-fitting the skin permeation profile of FL and FD-4 through hairless rat skin and LSE-high.

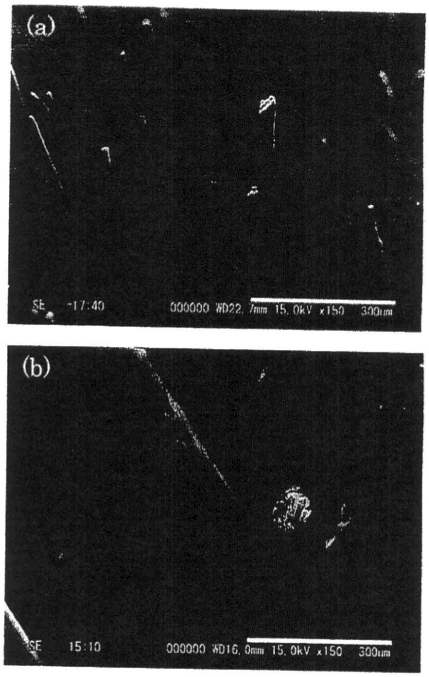

Fig. 5. SEM Observation of Hairless Rat Skin (a) and Porcine Ear Skin (b)

Bar=300 μm.

Increased partition and diffusion parameters of FL in hairless rat skin might mean that FL was mainly partitioned in pore routes and permeated the pore routes of skin; therefore, skin appendages, such as hair follicles, are the predominant permeation route of FL.

The diffusion parameters of FL and FD-4 in hairless rat skin showed almost the same value due to the slight difference in the cubic root of the molecular weight of these compounds, because the diffusion coefficient is proportional to the reciprocal of the cubic root, which is given by the Stokes–Einstein equation. Therefore, FL and FD-4 must permeate through almost the same permeation pathway of skin. On the other hand, the partition parameter of FD-4 was about one-third that of FL, indicating that FD-4 permeated skin through a more restricted pathway, such as hair follicles, than the FL pathway. In addition to this assumption, the present fluorescence images strongly supported the skin appendage route as a useful pathway for skin permeation and/or the distribution of such macromolecular compounds.

Fluoresbrite did not permeate hairless rat skin or LSE-high. Thus, porcine skin was selected to observe its skin distribution because the pores of hair follicles in porcine skin

are larger than in hairless rat skin (see Fig. 5). Fluoresbrite was especially observed in the infundibulum of hair follicles of porcine skin and no spheres were observed more than 100-μm depth from the skin surface (Fig. 4). It is reasonable that Fluoresbrite was detected only in the hair follicle because even FD-4, having a smaller molecular radius than nanospheres, was mainly detected in hair follicles.

This indicated that hair follicles are expected to be a useful pathway, not only for macromolecular compounds, but also nanospheres, through the skin barrier. Scheuplein[18] reported that the contribution of the transappendage route to the skin permeation of low molecular compounds must be very low, although the transfollicular pathway would play a very important role in the early stage of skin permeation and distribution. This is because the skin appendage area is only 0.1% of the total skin surface area.[18,24] Further study is necessary to fully elucidate the contribution of hair follicles to the skin permeation or distribution of hydrophilic compounds and nano-/microspheres. This contribution of hair follicles can be assessed using skin permeation parameters, such as $\varepsilon \cdot L$ and $D/\tau \cdot L^2$ as above.

CONCLUSION

The present study revealed that important role of hair follicles as a permeation pathway or distribution pathway for hydrophilic compounds and nanospheres. Although not only skin features, such as hair density and follicle size, but also physicochemical properties, such as molecular size and *n*-octanol/water partition coefficient of compounds, affect their transfollicular permeation,[25] analysis of the hair follicle contribution to the overall skin permeation of compounds using permeation parameters will help to understand efficient compound targeting of hair follicles.

Acknowledgement This study was supported by a Grant-in-Aid for Scientific Research (H20-iyaku-ippan-001) from the Ministry of Health, Labor, and Welfare, Japan.

REFERENCES

1) Ravi Kumar M. N., *J. Pharm. Pharm. Sci.*, **3**, 234—258 (2000).
2) Bilati U., Allemann E., Doelker E., *Eur. J. Pharm. Biopharm.*, **59**, 375—388 (2005).
3) Takeuchi H., Matsui Y., Sugihara H., Yamamoto H., Kawashima Y., *Int. J. Pharm.*, **303**, 160—170 (2005).
4) Todo H., Iida K., Okamoto H., Danjo K., *J. Pharm. Sci.*, **92**, 2475—2486 (2003).
5) Alvarez-Roman R., Naik A., Kalia Y. N., Guy R. H., Fessi H., *J. Controlled Release*, **99**, 53—62 (2004).
6) Almeida A. J., Souto E., *Adv. Drug Deliv. Rev.*, **59**, 478—490 (2007).
7) Honeywell-Nguyen P. L., Wouter Groenink H. W., Bouwstra J. A., *J. Liposome Res.*, **16**, 273—280 (2006).
8) Bos J. D., Meinardi M. M., *Exp. Dermatol.*, **9**, 165—169 (2000).
9) Lademann J., Weigmann H., Rickmeyer C., Barthelmes H., Schaefer H., Mueller G., Sterry W., *Skin Pharmacol. Appl. Skin Physiol.*, **12**, 247—256 (1999).
10) Toll R., Jacobi U., Richter H., Lademann J., Schaefer H., Blume-Peytavi U., *J. Invest. Dermatol.*, **123**, 168—176 (2004).
11) Trauer S., Patzelt A., Otberg N., Knorr F., Rozycki C., Balizs G., Buttemeyer R., Linscheid M., Liebsch M., Lademann J., *Br. J. Clin. Pharmacol.*, **68**, 181—186 (2009).
12) Teichmann A., Jacobi U., Ossadnik M., Richter H., Koch S., Sterry W., Lademann J., *J. Invest. Dermatol.*, **125**, 264—269 (2005).
13) Mota M. C., Carvalho P., Ramalho J., Leite E., *Int. Ophthalmol.*, **15**, 321—326 (1991).
14) Watanabe T., Hasegawa T., Takahashi H., Ishibashi T., Takayama K., Sugibayashi K., *Altern. Animal Test Experiment.*, **8**, 1—14 (2001).
15) Okumura M., Sugibayashi K., Ogawa K., Morimoto Y., *Chem. Pharm. Bull.*, **37**, 1404—1406 (1989).
16) Obata Y., Takayama K., Maitani Y., Machida Y., Nagai T., *Biol. Pharm. Bull.*, **16**, 312—314 (1993).
17) Sugibayashi K., Hosoya K., Morimoto Y., Higuchi W. I., *J. Pharm. Pharmacol.*, **37**, 578—580 (1985).
18) Scheuplein R. J., *J. Invest. Dermatol.*, **48**, 79—88 (1967).
19) Sugibayashi K., Hayashi T., Matsumoto K., Hasegawa T., *Drug Metab. Pharmacokinet.*, **19**, 352—362 (2004).
20) Sato K., Sugibayashi K., Morimoto Y., *J. Pharm. Sci.*, **80**, 104—107 (1991).
21) Scientific Committee on Consumer Product, "Opinion on Safety on Nanomaterials in Cosmetic Products," 2007.
22) Lauer A. C., Lieb L. M., Ramachandran C., Flynn G. L., Weiner N. D., *Pharm. Res.*, **12**, 179—186 (1995).
23) Okamoto H., Yamashita F., Saito K., Hashida M., *Pharm. Res.*, **6**, 931—937 (1989).
24) Ogiso T., Shiraki T., Okajima K., Tanino T., Iwaki M., Wada T., *J. Drug Target.*, **10**, 369—378 (2002).
25) Knorr F., Lademann J., Patzelt A., Sterry W., Blume-Peytavi U., Vogt A., *Eur. J. Pharm. Biopharm.*, **71**, 173—180 (2009).

The Journal of Toxicological Sciences (J. Toxicol. Sci.)
Vol.36, No.1, 95-100, 2011

Letter

Effects of coating materials and size of titanium dioxide particles on their cytotoxicity and penetration into the cellular membrane

Tadashi Uchino, Yoshiaki Ikarashi and Tetsuji Nishimura

Division of Environmental Chemistry, National Institute of Health Sciences, 1-18-1 Kamiyoga, Setagaya-ku, Tokyo 158-8501, Japan

(Received August 6, 2010; Accepted October 15, 2010)

ABSTRACT — In order to estimate the effects of the size and surface treatment (coating or non-coating) of titanium dioxide particles on their cytotoxicity and penetration into the cellular membrane, two types of non-treated titanium dioxide (TiO_2) particles of 20 nm (LU175) and 250 nm (LU205) were exposed to CHO cells, RBL-2H3 cells, A431 cells, B16 melanoma, NHEK(F), and NHSF, and six types of surface-treated or non-treated TiO_2 particles of 35 nm were exposed to RBL-2H3 cells and NHSF. The order of half-maximal inhibitory concentrations (IC50s) of LU175 was NHSF < CHO, RBL-2H3 < A431 < B16 melanoma, NHEK(F). On the other hand, LU205 showed no cytotoxicity against any cells. Surface-treated TiO_2 showed much less cytotoxicity against RBL-2H3 cells than non-treated TiO_2. Then, between 0.5 and 10 mg of LU175 or LU205 was exposed to CHO cells. After 24 hr, the amount of LU175 in cellular cytosol increased dose-dependently. On the other hand, the amount of LU205 in cellular cytosol was much less than that of LU175. The proportion of surface-treated TiO_2 in the cellular cytosol of RBL-2H3 cells differed for each coating material. These results suggested that TiO_2 has different cytotoxicities among cell lines, and that of surface-treated TiO_2 was weaker than that of non-treated TiO_2. TiO_2 located in cytosol might be the main cause of cytotoxicity.

Key words: Nanomaterials, Titanium dioxide, Cytotoxicity, Penetration, RBL-2H3 cells, NHSF

INTRODUCTION

In recent years, the use of nanomaterials such as titanium dioxide (TiO_2) in cosmetics such as sunscreen has advanced rapidly without adequate evaluation of their safety (Ishii, 2005; Hatakeyama, 2005; Lovern and Klaper, 2006; Xia *et al.*, 2006). Hussain *et al.* (2005) demonstrated that TiO_2 (40 nm) at higher doses (100-250 μg/ml) did not induce significant cytotoxicity against BRL 3A rat liver cells, while silver nanoparticles at lower doses (10-50 μg/ml) induced significant cytotoxicity against the cells. Reeves *et al.* (2008) demonstrated that TiO_2 (anatase, 5 nm) at 1,000 μg/ml induced slight cytotoxicity against goldfish skin cells without Ultraviolet-A(UVA)-irradiation. On the other hand, Sayes *et al.* (2006) demonstrated that nanoscale TiO_2 at 100 μg/ml induced significant cytotoxicity and inflammation against human dermal fibroblasts and human lung epithelial cells. Onuma *et al.* (2009) demonstrated that nano-sized TiO_2 had strong cytotoxicity against mouse fibrosarcoma cells. However, few reports about cytotoxicity of nano-sized TiO_2. In particular, little is known about cytotoxicity of nano-sized TiO_2 against various kinds of cells. Thus, it was considered necessary to compare cytotoxicity of nano-sized TiO_2 among various kinds of cells to estimate the potential toxicity of TiO_2. In order to estimate the toxicity of TiO_2, we examined the cytotoxicity of two kinds of non-coating rutile form TiO_2 with particle sizes of 20 nm (LU175) and 250 nm (LU205) against various kinds of cells and transferred LU175 and LU205 into the cellular components.

Surfaces of TiO_2 are usually coated with SiO_2, $Al(OH)_3$, Al_2O_3, or silicone for use in cosmetics. Warheit *et al.* (2007) demonstrated that surface-treated material affects TiO_2 toxicity against rat lung. However, there are few reports investigating the cytotoxic effects of coating materials on cells and the penetration of TiO_2 into cellular components. We examined the cytotoxicity of surface-treated and non-treated TiO_2 against cultured cells and

Correspondence: Tadashi Uchino (E-mail: uchino@nihs.go.jp)

transferred TiO_2 into the cellular components.

MATERIALS AND METHODS

Cells

C57BL/6 mouse melanoma (B16 melanoma), Chinese hamster ovary (CHO) cells, and rat basophilic leukemia (RBL-2H3) cells were purchased from Health Science Research Resources Bank (Osaka, Japan). Normal human skin fibroblasts (NHSF) and human epidermoid carcinoma (A431) cells were purchased from Riken Bioresources Center Cell Bank (Ibaraki, Japan). Normal human epidermis keratinocytes from neonatal foreskin (NHEK(F)) were purchased from Kurabo Industries Ltd. (Osaka, Japan).

Culture medium

Eagle's-MEM containing 10% FBS was used as culture medium for B16 melanomas, CHO cells and RBL-2H3 cells. Epi-Life KG2 was used as culture medium for A431 cells and NHEK(F). α-MEM containing 10% FBS was used as culture medium for NHSF.

Particles

Non-coating materials

LU175 and LU205 were obtained from Isihara Sangyo Kaisha, Ltd. (Osaka, Japan). TiO_2 (rutile form) particles of 35 nm (MT-500B; TiO_2 96%) were obtained from Teika Co. (Osaka, Japan).

Coating materials

TiO_2 (rutile form) particles of 35 nm coated with $Al(OH)_3$ and stearic acid (TTO-55(C); TiO_2 90%) and such particles coated with $Al(OH)_3$ (TTO-55(A); TiO_2 96%) were obtained from Isihara Sangyo Kaisha, Ltd. TiO_2 (rutile form) particles of 35 nm coated with $Al(OH)_3$, SiO_2, and silicone (SMT-500SAS; TiO_2 80%), such particles coated with $Al(OH)_3$ and SiO_2 (MT-500SA; TiO_2 85%), and such particles coated with Al_2O_3 (MT-500H; TiO_2 90%) were obtained from Teika Co.

Microwave digestion

After collecting cellular membrane, microsome, and cytosol, these components were added to teflon vessels, and then 5 ml of HNO_3 was added to each vessel. Then, the vessel contents were digested for 22 min (up to 80 PSI for 20 min, maintained for 2 min) using a microwave (MARS 5, CEM Co., Matthews, NC, USA).

ICP-MS measurement

The digested solution was diluted 5 times with milli-Q water and Ti contents were determined by ICP-MS (HP-4500, Hewlett-Packard Co., Palo Alto, CA, USA). ICP-MS conditions were as follows:

RF power:1450 W, RF refraction current: 5 W

Monitoring mass: m/z 48 (Ti)

Cytotoxicity

B16 melanomas, CHO cells, and RBL-2H3 cells were suspended in 0.1 ml of culture medium at a concentration of 5×10^4 cells/ml. A431 cells and NHEK(F) were suspended in 0.1 ml of culture medium at concentrations of 4×10^4 cells/ml and 5×10^4 cells/ml, respectively. NHSF was suspended in 0.1 ml of culture medium at a concentration of 4×10^4 cells/ml. All cells were seeded in a 96-well microplate and cultured for 2 days for CHO cells, 5 days for A431 cells, or 3 days for other cells under 5% CO_2 at 37°C.

TiO_2 particles were suspened in culture medium and ultrasonicated for 5 min. Immediately after ultrasonication, culture medium in the each microplate were removed and suspension (0.1 ml) of LU175 or LU205, the concentration of which ranged from 0 to 10 mg/ml, was added to each well. After 24 hr, cells were washed 5 times with medium and then for the viability assay, 0.1 ml of tetra-color one dissolved in medium was added, followed by incubation for 2 hr. Tetra -color one is a mixture of water-soluable tetrazolium solt [2-(2-Methoxy-4-nitrophenyl)-3-(4-nitorophenyl)-5-(2,4-disulfophenyl)-2H-tetrazolium, monosodium salt)] and electron carrier (1-Methoxy-5-methylphenazinium methylsulfate) converted to a water-soluable formazan by dehydrogenase enzymes located mainly in the mitochondria of living cells. Absorbance at 490 nm (reference at 650 nm) was measured with a microplate reader (Spectramax M5, Molecular Devices Co., Tokyo, Japan) and the half-maximal inhibitory concentration of viability (IC50) was derived.

TiO_2 transferred into cellular components

Five ml of cell suspension of CHO cells and RBL-2H3 cells (5×10^4 cells/ml) or NHSF cells (4×10^4 cells/ml) was cultured in a 60-mm dish for 2 days under 5% CO_2 at 37°C. After removing the medium, 5 ml of 0.1 or 0.5 or 2 mg/ml TiO_2 suspened in culture medium was added and the mixture was incubated for a further 24 hr. After washing cells 5 times with medium, the cells were treated with trypsin and collected. The cells were suspended in 1.5 ml of phosphate-buffered saline (PBS) and ultrasonicated for 5 min. Then, cell suspensions were cell-fractionated in accordance with the scheme shown in Fig.1 and the

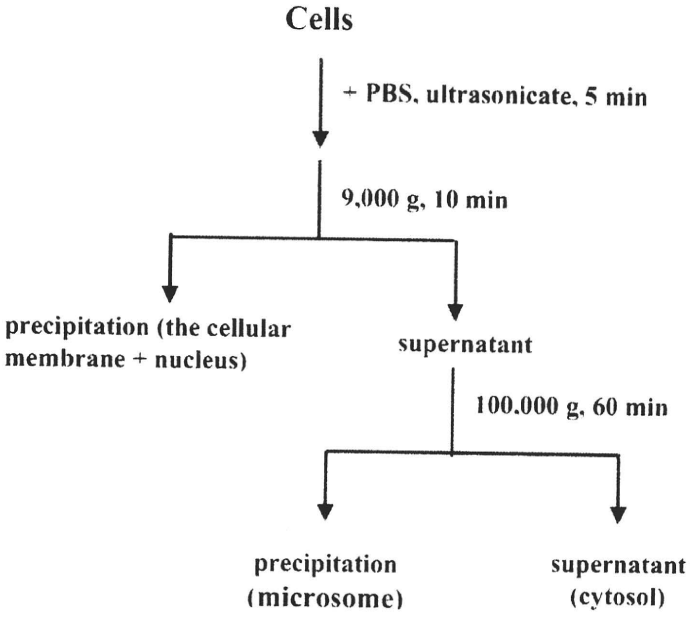

Fig. 1. Method of cell fractionation.

levels of Ti in the cellular membrane (including nucleus), microsome, and cytosol were determined by ICP-MS.

Statistical analysis

Differences between A431 and NHSF, CHO, or RBL-2H3 group, non-coated TiO_2 treatment group, and surface-treated TiO_2 treatment group were examined by Student's t-test. The differences were considered significant at $P < 0.05$.

RESULTS

Cytotoxicity of TiO_2 against cultured cells

LU175 showed cytotoxicity against NHSF, CHO, and RBL-2H3. On the other hand, LU175 showed no cytotoxicity against A431, B16 melanoma, and NHEK(F). IC50s of LU175 against NHSF, CHO, and RBL-2H3 were significantly decreased from that of the A431 group. LU205 showed no cytotoxicty against any cells (Table 1). IC50s of surface-treated TiO_2 were significantly higher than those of non-treated TiO_2 against NHSF and RBL-2H3 cells (Table 2).

Transfer of TiO_2 into the cellular components

500-10,000 μg of LU175 or LU205 was added to a culture of CHO cells in a 60-mm dish. After 24 hr, over 99% of LU205 was located in the cellular membrane, while 88.5-96.7% and 3.3-11.3% of LU175 were located in cellular membrane and cytosol, respectively (Table 3). The proportion of LU175 located in the cytosol was significantly increased from that in the LU205 group (Table 3).

The suspensions of 100 μg/ml surface-treated and non-treated TiO_2 were added to the NHSF seeded in a 60-mm dish. In non-treated TiO_2, proportions of MT-500B and LU175 located in cytosol were significantly increased from that in the LU205 group (Table 4). In surface-treated TiO_2, proportions of TTO-55(C) and SMT-500SAS located in cytosol were significantly increased from that in the MT-500SA group (Table 4). Similar results were obtained for RBL-2H3 cells (Table 4).

DISCUSSION

Xu *et al.* (2010) reported that nano-scale TiO_2 was administered to wild-type rat by a novel intrapulmonary spraying five times over 9 days. 8-hydroxyguanosine level and superoxide dismutase activity expression in the lung. Gurr *et al.* (2005) and Onuma *et al.* (2009) reported that reactive oxygen generated from TiO_2 in the dark induced cytotoxicity. Thus, the mechanism of the cytotoxicity of LU175 might be through reactive oxygen generated from TiO_2 in the dark. However, it was not clear that the kind of reactive oxygen generated from TiO_2 in the dark. Therefore, further study should be carried out.

Table 1. Cytotoxicity of LU175 and LU205 against various cells

Cell	IC50 (mg/ml)	
	LU175	LU205
CHO	1.3 ± 0.3*	> 10
RBL-2H3	1.4 ± 1.0*	8.6 ± 1.2
NHSF	0.5 ± 0.2**	> 10
A431	8.3 ± 2.9	7.0 ± 2.6
NHEK (F)	> 10	> 10
B16 melanoma	> 10	> 10

Data are means ± S.D. of three experiments. Significantly different from A431 group, *P < 0.05, **P < 0.01.

Table 2. Cytotoxicity of TiO_2 against NHSF and RBL-2H3 cells

	IC50 (mg/ml)	
	NHSF	RBL-2H3
SMT-500SAS	4.6 ± 0.4***	4.9 ± 1.9*
MT-500SA	> 10	> 10
MT-500H	> 10	5.9 ± 1.4**
TTO-55 (C)	2.1 ± 1.5	2.3 ± 1.4
TTO-55 (A)	> 10	> 10
MT-500B	0.12 ± 0.04	0.6 ± 0.4

Data are means ± S.D. of three experiments. Significantly different from MT-500B group, *P < 0.05, **P < 0.01, ***P < 0.001.

Table 3. The distribution of different particle sizes of TiO_2 in the cellular components of CHO cells

	Exposed (μg)	Detected (μg: mean ± S.D. n = 3)		
		Membrane	Microsome	Cytosol
LU175	500	83 ± 3	ND (< 0.004)	4.1 ± 2.7
		(95.3 ± 3.4%)	(0.0%)	(4.7 ± 3.1%)
	2500	176 ± 15	ND	6.0 ± 2.4*
		(96.7 ± 8.2%)	(0.0%)	(3.3 ± 1.3%*)
	10000	133 ± 17	0.28 ± 0.12	17 ± 14
		(88.5 ± 11.3%)	(0.2 ± 0.08%)	(11.3 ± 9.3%)
LU205	500	416 ± 8	2.4 ± 0.7	0.050 ± 0.001
		(99.41 ± 1.91%)	(0.57 ± 0.17%)	(0.02 ± 0.0004%)
	2500	1238 ± 25	3.6 ± 1.1	0.05 ± 0.08
		(99.71 ± 2.01%)	(0.29 ± 0.09%)	(0.004 ± 0.007%)
	10000	5395 ± 836	0.28 ± 0.11	0.61 ± 0.08
		(99.98 ± 15.49%)	(0.005 ± 0.002%)	(0.01 ± 0.001%)

The data detected after 24-hr exposure of TiO_2 onto CHO cells. Significantly different from LU205 group, *P < 0.05

The cell size of NHSF, CHO, and RBL-2H3 cells were larger than B16 melanoma, A431 cells, and NHEK(F). Therefore, it was speculated that the cytotoxicity of LU175 might be connected to cell size. Surface-treated TiO_2 showed less cytotoxicity against RBL-2H3 cells and NHSF than non-treated TiO_2.

These results suggested that surface treatment with coating materials would reduce the surface reactive activity of TiO_2 and thus reduce its cytotoxicity. On the other hand, the cytotoxicity of surface-treated TiO_2 depends on the kind of coating material. The cytotoxicities of coating materials themselves are not known, so further study should be carried out.

Dose-dependent levels of LU175 were present in the cytosol of CHO cells. MT-500B and LU175 located in the cytosol of NHSF and RBL-2H3 cells were significantly increased from those in the LU205 group (Tables 3 and 4).

These results suggested that non-coating TiO_2 locat-

Table 4. Influence of surface coating on the distribution of TiO_2 in the cellular components of NHSF and RBL-2H3 cells

(a) NHSF

(unit: μg)

TiO_2 500 μg	SMT-500SAS	MT-500SA	MT-500H	TTO-55(C)	TTO-55(A)	MT-500B	LU175	LU205
Cellular membrane	15.8 ± 1.4	11.7 ± 4	68.5 ± 3.8	3.55 ± 0.04	76.0 ± 2.3	83.2 ± 4.7	84 ± 5	426 ± 26
Microsome	0.26 ± 0.17	3.89 ± 0.26	0.92 ± 0.20	1.88 ± 0.06	ND	2.64 ± 0.24	23 ± 13	ND
Cytosol	1.92 ± 0.11	0.43 ± 0.04	2.85 ± 0.18	2.98 ± 0.18	0.59 ± 0.01	0.72 ± 0.07	2.8 ± 1.6	1.0 ± 0.7

(mean ± S.D., n = 3)

(presence ratio: %)

TiO_2 500 μg	SMT-500SAS	MT-500SA	MT-500H	TTO-55(C)	TTO-55(A)	MT-500B	LU175	LU205
Cellular membrane	87.88 ± 7.78	96.44 ± 3.30	94.78 ± 5.26	42.2 ± 0.5 ###	99.23 ± 3.00	96.11 ± 5.43	76.4 ± 4.6**	99.8 ± 6.1
Microsome	1.45 ± 0.95	3.21 ± 0.21	1.27 ± 0.28	22.4 ± 0.7	ND	3.05 ± 0.27	20.9 ± 11.8	ND
Cytosol	10.67 ± 0.61 ###	0.35 ± 0.03	3.95 ± 0.25	35.4 ± 2.1 ###	0.77 ± 0.01	0.84 ± 0.08**	2.5 ± 1.5	0.20 ± 0.16

(mean ± S.D., n = 3)

(b) RBL-2H3

(unit: μg)

TiO_2 500 μg	SMT-500SAS	MT-500SA	MT-500H	TTO-55(C)	TTO-55(A)	MT-500B	LU175	LU205
Cellular membrane	36.9 ± 18.7	283 ± 63	116 ± 48	32.0 ± 22.2	73.9 ± 5.8	89.3 ± 23.3	383 ± 39	471 ± 71
Microsome	0.24 ± 0.12	3.1 ± 1.5	1.3 ± 0.3	0.18 ± 0.27	0.91 ± 0.41	0.53 ± 0.17	3.1 ± 0.4	6.1 ± 0.6
Cytosol	0.63 ± 0.08	1.10 ± 0.06	3.61 ± 0.14	1.17 ± 0.09	0.86 ± 0.03	0.79 ± 0.06	0.54 ± 0.11	0.17 ± 0.13

(mean ± S.D., n = 3)

(presence ratio: %)

TiO_2 500 μg	SMT-500SAS	MT-500SA	MT-500H	TTO-55(C)	TTO-55(A)	MT-500B	LU175	LU205
Cellular membrane	97.7 ± 49.5	98.54 ± 21.94	95.94 ± 39.70	95.95 ± 66.57	97.66 ± 7.66	98.54 ± 25.71	99.05 ± 10.09	98.69 ± 14.88
Microsome	0.64 ± 0.32	1.08 ± 0.52	1.08 ± 0.25	0.54 ± 0.81	1.22 ± 0.54	0.58 ± 0.32	0.81 ± 0.10	1.27 ± 0.13
Cytosol	1.66 ± 0.21 ###	0.38 ± 0.02	2.98 ± 0.12	3.51 ± 0.27 ###	1.14 ± 0.04	0.87 ± 0.07***	0.14 ± 0.03*	0.04 ± 0.03

(mean ± S.D., n = 3)

Significantly different from LU205 group, *P < 0.05, **P < 0.01, ***P < 0.001
Significantly different from MT-500SA group, ###P < 0.001

ed in the cytosol might be the main cause of cytotoxicity. Since the distribution in the cytosol of surface-treated TiO_2 is at the same level or higher than that of non-coating TiO_2, the distribution in the cytosol of surface-treated TiO_2 might not be the cause of the cytotoxicity of TiO_2. Since the distributions in the cytosol of TTO-55(C) and SMT-500SAS were significantly increased from that in the MT-500SA group, stearic acid or silicone induced the distribution in the cytosol.

ACKNOWLEDGMENTS

We thank Isihara Sangyo Kaisha, Ltd. for generously donating LU175, LU205, TTO-55(C), and TTO-55(A) and Teika Co. for generously donating MT-500B, SMT-500SAS, MT-500SA, and MT-500H.

REFERENCES

Gurr, J., Wang, A.S.S., Chen, C. and Jan, K. (2005): Ultrafine titanium dioxide particles in the absence of photoactivation can induce oxidative damage to human bronchial epithelial cells. Toxicology, **213**, 66-73.

Hatakeyama, Y. (2005): Safety evaluation of the nanoparticles on cosmetics. Journal of Japanese Cosmetic Science Society, **29**, 225-231.

Hussain, S.M., Hess, K.L., Gearhart, J.M., Geiss, K.T. and Schlager, J.J. (2005): *In vitro* toxicity of nanoparticles in BRL 3A rat liver cells. Toxicol. In Vitro, **19**, 975-983.

Ishii, H. (2005): Development of water resistant sunscreening agent using nano-technology. Journal of Japanese Cosmetic Science Society, **29**, 215-220.

Lovern, S.B. and Klaper, R. (2006): Daphnia magna mortality when exposed to titanium dioxide and fullerene (C60) nanoparticles. Environmental Toxicol. Chem., **25**, 1132-1137.

Onuma, K., Sato, Y., Ogawara, S., Shirasawa, N., Kobayashi, M., Yoshitake, J., Yoshimura, T., Iigo, M., Fujii, J. and Okada, F. (2009): Nano-scaled particles of titanium dioxide convert benign mouse fibrosarcoma cells into aggressive tumor cells. Am. J. Pathol., **175**, 2171-2183.

Reeves, J.F., Davies, S.J., Dodd, N.J. and Jha, A.N. (2008): Hydroxyl radicals ($^{\cdot}OH$) are associated with titanium dioxide (TiO_2) nanoparticle-induced cytotoxicity and oxidative DNA damage in fish cells. Mutat. Res., **640**, 113-122.

Sayes, C.M., Wahi, R., Kurian, P.A., Liu, Y., West, J.L., Ausman, K.D., Warheit, D.B. and Colvin, V.L. (2006): Correlating nanoscale titania structure with toxicity: a cytotoxicity and inflammatory response study with human dermal fibroblasts and human lung epithelial cells. Toxicol. Sci., **92**, 174-185.

Warheit, D.B., Webb, T.R., Reed, K.L., Frerichs, S. and Sayes, C.M. (2007): Pulmonary toxicity study in rats with three forms of ultrafine-TiO_2 particles: differential responses related to surface properties. Toxicology, **230**, 90-104.

Xia, T., Kovochich, M., Brant, J., Hotze, M., Sempf, J., Oberley, T., Sioutas, C., Yeh, J.I., Wiesner, M.R. and Nel, A.E. (2006): Comparison of the abilities of ambient and manufactured nanoparticles to induce cellular toxicity according to an oxidative stress paradigm. Nano Lett., **6**, 1794-1807.

Xu, J., Futakuchi, M., Iigo, M., Fukamachi, K., Alexander, D.B., Shimizu, H., Sakai, Y., Tamano, S., Furukawa, F., Uchino, T., Tokunaga, H., Nishimura, T., Hirose, A., Kanno, J. and Tsuda, H. (2010): Involvement of macrophage inflammatory protein 1α(MIP1α) in promotion of rat lung and mammary carcinogenic activity of nanoscale titanium dioxide particles administered by intra-pulmonary spraying. Carcinogenesis, **31**, 927-935.

Enhancement of tongue carcinogenesis in Hras128 transgenic rats treated with 4-nitroquinoline 1-oxide

KUNIKO NAOI[1], NAO SUNAGAWA[2], ICHIRO YOSHIDA[1], TAKAMITSU MORIOKA[2], MAKOTO NAKASHIMA[1], MASASHI ISHIHARA[1,3], KATSUMI FUKAMACHI[4], YOSHINORI ITOH[3], HIROYUKI TSUDA[4], NAOKI YOSHIMI[2] and MASUMI SUZUI[1]

[1]Department of Medical Therapeutics and Molecular Therapeutics, Gifu Pharmaceutical University, 5-6-1 Mitahora-higashi, Gifu 502-8585; [2]Tumor Pathology Division, University of the Ryukyus Faculty of Medicine, 207 Uehara, Nishihara-cho, Okinawa 903-0215; [3]Department of Pharmacy, Gifu University Hospital, 1-1 Yanagido, Gifu 501-1194; [4]Department of Molecular Toxicology, Graduate School of Medical Sciences, Nagoya City University, 1 Kawasumi, Mizuho-cho, Mizuho-ku, Nagoya 467-8601, Japan

Received September 3, 2009; Accepted October 29, 2009

DOI: 10.3892/or_00000641

Abstract. Transgenic rats carrying human c-Ha-*ras* proto-oncogene (Hras128 rats) have been shown to be highly susceptible to induction of tumors. We have found an early induction of tongue tumors in Hras128 rats treated with 4-nitroquinoline 1-oxide (4NQO). 4NQO was administered to the Hras128 and wild-type Sprague-Dawley (SD) rats for 4 and 8 weeks, respectively. The experiment was terminated at 14 (Hras128 rats) and 28 (SD rats) weeks. Either during or after treatment with 4NQO, dysplastic hyperplasia, papilloma and squamous cell carcinoma were found on the tongue of both Hras128 and wild-type rats, with a higher incidence and multiplicity in Hras128 rats. Treatment of the Hras128 rats with 4NQO significantly increased cell proliferation in the tumor compared to the control rats. In the tongue tumors of the Hras128 rats, there was a significant increase in the mRNA expression levels of cyclin D1 and COX2. To examine whether this experimental system is useful for screening of the candidate agents for cancer preventive effect, nimesulide, a selective COX2 inhibitor, was tested in the present model. Nimesulide significantly decreased total multiplicity of tongue lesions compared to the control rats. Treatment of Hras128 rats with nimesulide caused a significant decrease in the levels of mRNA expression of cyclin D1 and COX2 in the tumor. Therefore, the current 4NQO-induced Hras128 rat tongue carcinogenesis model provides a simple and rapid system for investigating carcinogenesis process and evaluating the effect of possible cancer preventive agents for human tongue cancer.

Correspondence to: Dr Masumi Suzui, Department of Medical Therapeutics and Molecular Therapeutics, Gifu Pharmaceutical University, 5-6-1 Mitahora-higashi, Gifu 502-8585, Japan
E-mail: suzui@gifu-pu.ac.jp

Key words: tongue carcinogenesis, *ras*, transgenic rat, 4-nitroquinoline 1-oxide

Introduction

Oral cancer is a relatively common malignancy ranking 11th in frequency on a worldwide basis, and more than 390,000 new cases are being diagnosed annually (1,2). Human oral cancer is related to cigarette smoking and chewing or smokeless tobacco (3). This disease has a multifocal character often referred to as a field cancerization (4). This malignancy is most common in developing countries of Asia and South America (5), and incidence and mortality rate of this disease are rising in developed countries, especially in young males (6-8). This aggressive epithelial malignancy is associated with severe morbidity and poor survival despite recent advances in treatment (7).

Rat model using 4-nitroquinoline 1-oxide (4NQO) has been widely used for investigating carcinogenesis of oral cancer and evaluating the modulatory effects of possible chemopreventive agents (9,10). The 4NQO-induced oral cancer is derived from papilloma through hyperplastic epithelium and dysplasia (11), and this multistage process mimics the development of these malignancies in human (11,12). Recent reports by Tsuda and his colleagues demonstrate that transgenic rat carrying human c-Ha-*ras* proto-oncogene, termed Hras128 rat [Jcl/SD-TgN(HrasGen)128Ncc], is highly susceptible to tumor induction in various organ sites including mammary gland, esophagus, skin, urinary bladder and tongue (13-15).

In the present study, we developed a novel tongue carcinogenesis Hras128 rat model by using 4NQO to cause a rapid induction of tongue tumors within as short a period as 14 experimental weeks. Using this experimental system, we also confirmed that nimesulide, a selective COX2 inhibitor, which has been demonstrated to prevent rat tongue carcinogenesis (16), prevents the occurrence of tongue tumors induced with 4NQO.

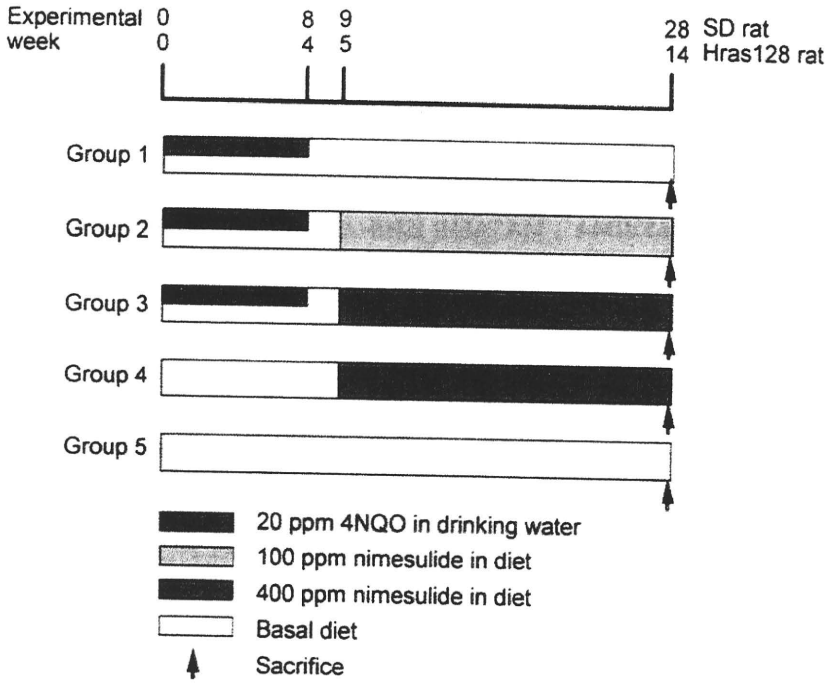

Figure 1. Experimental protocol. As indicated, the experimental period of the Hras128 and wild-type SD rat lasted 14 and 28 weeks, respectively.

Materials and methods

Animals. A total of 80 male Hras128 rats [Jcl/SD-TgN (HrasGen)128Ncc] and wild-type Sprague-Dawley (SD) rats bred by CLEA (CLEA Japan, Inc., Tokyo, Japan) at 6 weeks old were maintained in plastic cages in a conditioned room at 23±2°C, 50±10% humidity and 12-h light/dark cycle lighting. The animals were allowed free access to powdered basal diet CE-2 (CLEA Japan) and tap water. The animals were also maintained in the Animal Facility of University of the Ryukyus, Faculty of Medicine, and the experiments were conducted according to the Institutional Animal Care Guidelines of University of the Ryukyus.

Treatment. After one week of acclimatization, rats were randomly assigned to the experimental groups (Fig. 1). Hras128 and SD rats in groups 1-3 (10 rats each) were given tap water containing 20 ppm 4NQO (CAS no. 56-57-5, Wako Pure Chemical, Osaka, Japan; 98% pure) for 4 and 8 weeks, respectively. One week after 4NQO treatment, rats in groups 2 and 3 received 100 and 400 ppm nimesulide (CAS no. 51803-78-2, Nacalai Tesque, Inc., Kyoto, Japan) in basal diet until the end of the experiment, and rats in group 1 received no further treatment and fed the basal diet. Rats in group 4 received the 400 ppm nimesulide diet without 4NQO treatment. Rats in group 5 were fed the basal diet alone and served as untreated controls. Careful observation of tongue lesions was done on a weekly basis until the end of the experiment. Animals were weighed weekly and consumption of the experimental diets was also recorded. Tongue lesions including dysplastic hyperplasia (DH), papilloma (PAP) and squamous cell carcinoma (SCC) were noted grossly for their location, number, and size, and tumor incidence and multiplicity were analyzed. At 14 and 28 weeks after the start of the experiment, Hras128 and SD rats were euthanized with CO_2 anesthesia, and then complete autopsies were performed with these animals. The identified tumors were carefully removed and cut into two segments. One segment of the tumor was immediately frozen in liquid nitrogen for reverse transcription-PCR (RT-PCR) analysis; the second segment was fixed in 10% buffered formalin and then processed for histopathological (hematoxylin and eosin staining) and immunohistochemical analyses. Oral lesions including dysplasia and neoplasia were diagnosed according to the criteria described elsewhere (17,18).

Immunohistochemical staining and measurement of PCNA positive index. These assays were performed using an established method as previously described by us (19). In brief, 4-μm thick paraffin sections were prepared to include the tongue tumor or adjacent normal mucosa. These sections were treated in 3% H_2O_2 for 20 min to block the endogenous peroxidase activity and then incubated with a primary antibody of proliferating cell nuclear antigen (PCNA) (1:50 dilution) (Dako Co., Ltd., Kyoto, Japan) at room temperature for 60 min. Sections were then stained using a Simple Stain kit (Nichirei, Tokyo, Japan) according to the manufacturer's instructions. PCNA was measured in cells consisting of the tongue tumor or normal mucosa. The PCNA positive index was determined by calculating the ratio of PCNA-positive nuclei/total number of nuclei counted as described by us (19). More than 300 cells were counted in each lesion.

Reverse transcription-PCR (RT-PCR) analysis. These assays were performed by established procedures (20). Snap-frozen

Table I. Body, liver, kidney and relative liver weights in Hras128 rats.

Group	Treatment	No. of rats	Body weight (g)	Liver weight (g)	Kidney weight (g)	Relative liver weight (g/100 gr body weight)
1	4NQO	10	597±30[a,b]	24.6±2.9[b]	4.7±0.4	4.1±0.3[b]
2	4NQO→100 ppm nimesulide	10	577±24	22.4±3.1	4.6±0.4	3.8±0.4
3	4NQO→400 ppm nimesulide	10	531±42[b]	24.8±2.7	4.6±0.5	4.6±0.4[b]
4	400 ppm nimesulide	5	588±20	26.0±2.8	4.8±0.5	4.4±0.4
5	None	5	625±60[b]	28.0±4.8[b]	5.2±0.1	4.4±0.6

[a]Mean ± SD. [b]Statistically significant.

Table II. Body, liver, kidney and relative liver weights in Sprague-Dawley rats.

Group	Treatment	No. of rats	Body weight (g)	Liver weight (g)	Kidney weight (g)	Relative liver weight (g/100 gr body weight)
1	4NQO	8	523±100[a,b]	19.7±5.9	3.7±0.5[b]	3.7±0.8
2	4NQO→100 ppm nimesulide	10	520±77[b]	20.6±4.5	3.9±0.6	3.9±0.6[b]
3	4NQO→400 ppm nimesulide	10	538±29[b]	17.5±3.5[b]	3.6±0.4	3.2±0.5[b]
4	400 ppm nimesulide	5	662±96[b]	24.4±7.1[b]	5.0±0.8[b]	3.6±0.8
5	None	5	558±68	18.1±2.9	3.4±0.3	3.2±0.5[b]

[a]Mean ± SD. [b]Statistically significant.

histopathologically verified tongue tumors were randomly chosen and total RNA was extracted for RT-PCR assays. Total RNA was isolated from frozen tissues using a TRIzol reagent (Invitrogen Life Technologies, Inc., Rockville, MD) as recommended by the manufacturer. cDNA was amplified from total RNA (100 ng) using a SuperScript III One-Step RT-PCR System (Invitrogen Life Technologies). PCR was conducted for 35 or 38 cycles in a Takara PCR Thermal Cycler SP TP-400 (Takara Bio, Inc., Tokyo, Japan). The primers used for amplification were as follows: cyclin D1-specific primer set, CD-1F (5'-CTG GCC ATG AAC TAC CTG GA-3') and CD-1R (5'-GTC ACA CTT GAT GAC TCT GG-3'); p53-specific primer set, P-2F (5'-CAG CGA CAG GGT CAC CTA AT-3') and P-3R (5'-GTG GAT AGT GGT ATA GTC GG-3'); $p21^{CIP1}$-specific primer set, C-3F (5'-CCT TAG CCT TCA TTC AGT GT-3') and C-4R (5'-GCC AGG ATC AGA AAC ACA GC-3'); $p27^{KIP1}$-specific primer set, K-2F (5'-CCG CCT GCA GAA ACC TCT TC-3') and K-2R (5'-TGG ACA CTG CTC CGC TAA CC-3'); cyclooxygenase-2 (COX2)-specific primer set, PT-4F (5'-TGG GCC ATG GAG TGG ACT TA-3') and PT-4R (5'-ATG AGC CTG CTG GTT TGG AA-3'). ß-actin-specific PCR products for the same RNA samples were simultaneously amplified and served as internal controls. Primers BA-F2 (5'-GGG TAT GGG TCA GAA GGA CT-3') and BA-R2 (5'-TGT AGC CAC GCT CGG TCA GG-3') were used for amplification of ß-actin. Each amplification cycle consisted of 0.5 min at 94°C for denaturing, 0.5 min at 55°C for primer annealing and 1 min at 72°C for extension. PCR products were analyzed by agarose gel electrophoresis and stained with ethidium bromide. The results were confirmed by repeating experiments.

Statistical analysis. Tumor incidence and multiplicity were compared between the Hras128 and SD rats, or between animals treated with nimesulide and those not treated with nimesulide. Tumor incidence was analyzed by χ^2 or Fisher's exact probability test, and tumor multiplicity was analyzed by Student's or Welch's t-test. Significance was established at $P<0.05$.

Results

General observation. A total of 78 Hras128 and SD rats survived at the end of the experiment. Two SD rats in group 1 died from unidentified cause. No macroscopic metastases were observed in any of 78 rats. Body, liver, kidney and relative liver weights are shown in Tables I and II. In Table I, the body weight of group 3 was significantly lower than that

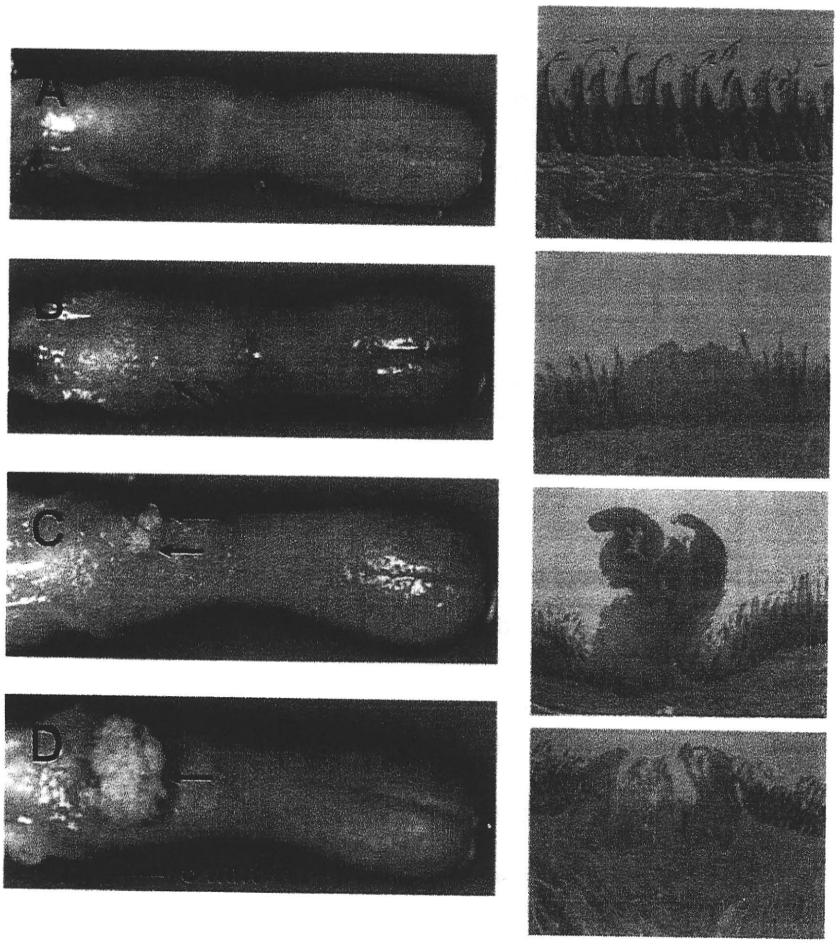

Figure 2. Macroscopic (left panels) and histological (right panels) appearance on the induced tongue lesions indicated by arrows. These lesions were induced with 4NQO in Hras128 rats. (A) Normal mucosa (N); (B) dysplastic hyperplasia (DH); (C) papilloma (PAP); (D) squamous cell carcinoma (SCC) (arrow). DH displayed thickened epithelium with prominent surface keratinization, loss of polarity in epithelial cells, nuclear pleomorphism, dyskeratosis and increased or abnormal mitosis. PAP and SCC exhibited non-invasive growth of neoplastic cells and invasive growth into subepithelial and muscular tissues, respectively.

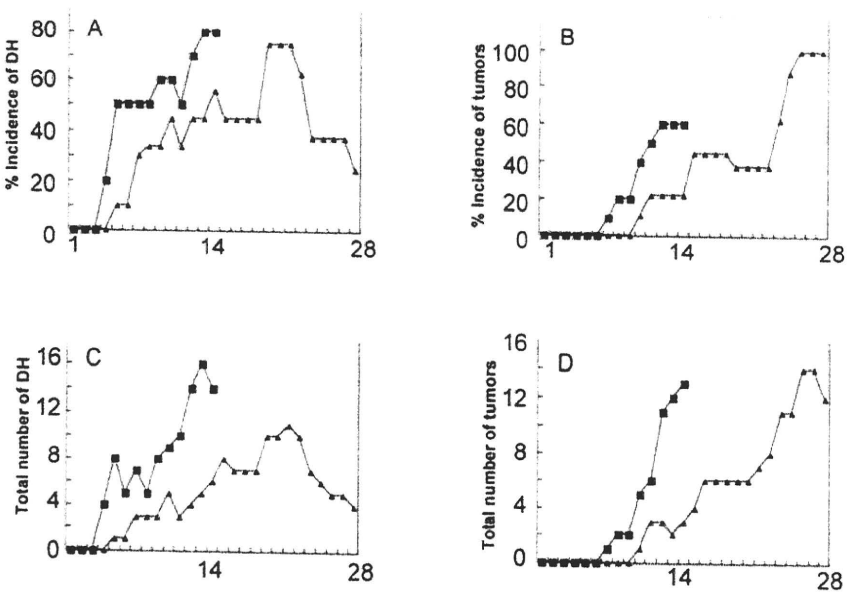

Figure 3. Occurrence of tongue lesions in Hras128 (closed square) and SD (closed triangle) rats. As indicated, left 2 panels indicate (%) incidence (A) and number (C) of dysplastic hyperplasia (DH). Note a marked increase in incidence and number of DH in Hras128 rats. This increase persisted until the end of the experiment (at experimental-week 14). Right 2 panels indicate (%) incidence (B) and number (D) of tumor. X-axis indicates the experimental week. Note that the incidence and number of tongue tumors (PAP and SCC) in the Hras128 rat are greater than that of the SD rat.

Table III. Incidence and multiplicity of the tongue lesions.

A. Hras128 rat

Group	Treatment	No. of rats	Incidence			Multiplicity		
			Total	DH	PAP+SCC	Total	DH	PAP+SCC
1	4NQO	10	8	8	6	3.4±2.1[a]	1.8±1.0	2.2±0.2
2	4NQO→100 ppm nimesulide	10	9	7	4	2.0±1.0	1.7±1.1	1.2±0.5
3	4NQO→400 ppm nimesulide	10	8	7	2[b]	1.6±0.7[c]	1.4±0.8	1.0±0.1
4	400 ppm nimesulide	5	0	0	0	0	0	0
5	None	5	0	0	0	0	0	0

[a]Mean ± SD. [b]Significantly different from group 1 by χ^2 test ($P<0.05$). [c]Significantly different from group 1 by Student's t-test ($P<0.05$). DH, dysplastic hyperplasia; PAP, papilloma; SCC, squamous cell carcinoma.

B. SD rat

Group	Treatment	No. of rats	Incidence			Multiplicity		
			Total	DH	PAP+SCC	Total	DH	PAP+SCC
1	4NQO	8	8	3	8	1.8±0.8[a]	2.0±1.4	1.5±0.8
2	4NQO→100 ppm nimesulide	10	10	2	8	1.6±0.7	1.3±0.6	1.5±0.8
3	4NQO→400 ppm nimesulide	10	10	2	8	1.3±0.7[b]	1.0±0.1	1.2±0.4
4	400 ppm nimesulide	5	0	0	0	0	0	0
5	None	5	0	0	0	0	0	0

[a]Mean ± SD. [b]Significantly different from group 1 by Student's t-test ($P<0.05$). DH, dysplastic hyperplasia; PAP, papilloma; SCC, squamous cell carcinoma.

of groups 1 ($P<0.001$) and 5 ($P<0.01$). Liver and relative liver weights of group 1 were significantly lower than that of groups 5 ($P<0.01$) and 3 ($P<0.01$), respectively. In Table II, the body weight of groups 1-3 was significantly lower than that of group 4 ($P<0.05$). Kidney and liver weights of group 1 and 3, respectively, were significantly lower than that of group 4 ($P<0.05$). Relative liver weight of group 2 was higher than that of groups 3 and 5 ($P<0.05$). These data indicate a toxic effect of 4NQO on the carcinogen-treated animals and that nimesulide may affect the weight of the body and the organs examined.

Occurrence of tongue lesions. On the time course study, an early induction of grossly visible tongue lesions including DH and tumor was found. These lesions were histopathologically DH, PAP and SCC (Fig. 2). After 3 weeks of 4NQO treatment, the incidence and number of DH in Hras128 rats markedly increased, and this increase persisted until the end of the experiment (at experimental-week 14) (Fig. 3A and C). In the DH lesion of Hras128 rats, treatment with 4NQO resulted in a 1.4- and 2.3-fold increase in incidence and number, respectively, when compared to the SD rats. At the experimental-week 14, the incidence and number of tongue tumors in the Hras128 rat were greater than that of the SD rat (Fig. 3B and D). Also, treatment of Hras128 rats with 4NQO resulted in a 2.7- and 4.3-fold increase in tumor incidence and number, respectively, when compared to the SD rats. At the end of the experiment, there was a significant increase in tumor multiplicity of the Hras128 rat (2.2±0.2) in comparison to the SD rat (1.5±0.8) ($P<0.05$). No visible esophageal tumors were found in any group of the Hras128 and SD rats.

Incidence and multiplicity of the tongue lesions. Treatment of Hras128 rats with 400 ppm nimesulide caused a significant and dose-dependent decrease in tumor incidence and total tumor multiplicity compared to group 1 ($P<0.05$, Table IIIA). In SD rats, the total tumor multiplicity was significantly decreased at 400 ppm nimesulide treatment ($P<0.05$, Table IIIB). In treatment of Hras128 and SD rats with nimesulide, the incidence and multiplicity were decreased in value but these changes were not statistically significant (Table III).

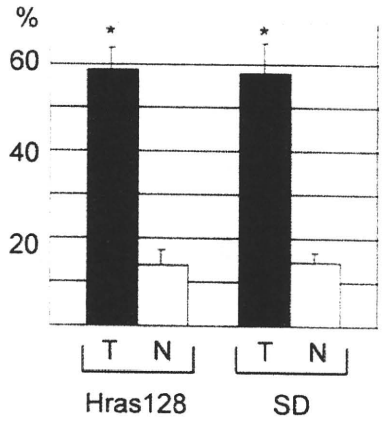

Figure 4. Proliferating cell nuclear antigen (PCNA) positive index in the tumor (T) and normal (N) tongue mucosa. Asterisks indicate significant difference in PCNA positive index between tumor and normal mucosa (Student's t-test, P<0.05). The difference was seen in both Hras128 and SD rats.

Positive index. To examine the effect of 4NQO in cell proliferation, we measured PCNA positive index in the tumor of group 1 and normal mucosa of group 5 (Fig. 4). In Hras128 rats, PCNA positive index was 58.8±4.9 (tumor) and 13.8±3.0 (normal mucosa). In SD rats, PCNA positive index was 58.1±6.6 (tumor) and 14.3±2.2 (normal mucosa). As shown in Fig. 4, treatment of Hras128 and SD rats with 4NQO caused a significant increase in PCNA positive index (P<0.05). These results indicate that treatment of rats with 4NQO increased cell proliferation in the tumor.

mRNA expression levels in the tumor of Hras128 rats. Because we found that at sacrifice the Hras128 rat developed greater number of tongue tumors than the SD rat and that 4NQO treatment enhanced cell proliferation in the tumor, we analyzed the levels of expression of cyclin D1, $p21^{CIP1}$, $p27^{KIP1}$, p53, COX2, using quantitative reverse transcription PCR (RT-PCR) assays. In tumor samples of the Hras128 rat, there was a marked (6.5- to 7.5-fold) and significant increase in the cellular levels of cyclin D1 and COX2 mRNA compared to the adjacent normal mucosa samples (Fig. 5). There was also a slight (1.7- to 2.3-fold) increase in those of p53 and $p21^{CIP1}$ mRNA (Fig. 5). We then examined whether nimesulide affects the levels of expression of these molecules in the tumors of Hras128 rats. Nimesulide caused a marked decrease in the cellular level of COX2, and also caused a slight decrease in that of cyclin D1 mRNA. Nimesulide treatment at high dose (400 ppm) inhibited the expression of COX2 mRNA to almost zero level. Nimesulide also caused a slight decrease in the cellular level of cyclin D1 mRNA.

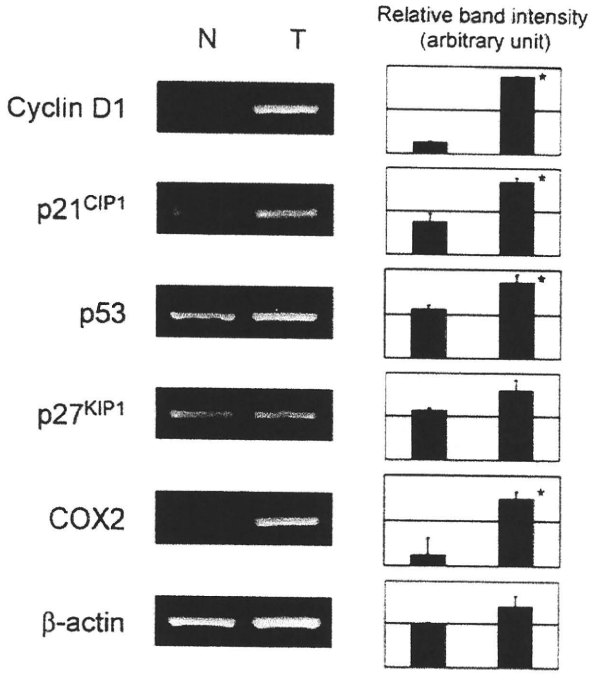

Figure 5. Representative results of RT-PCR assays. Densitometric analysis (right panel). Asterisks indicate significant difference between tumor (T) and adjacent normal mucosa (N) (P<0.05).

Discussion

Treatment of Hras128 rats with 4NQO caused an early induction (up to six experimental weeks) of DH and tumor in the tongue, when compared to the wild-type SD rat (Table III and Fig. 3). These results clearly show that Hras128 rats are more sensitive to 4NQO induced tongue carcinogenesis than SD rats. This susceptibility to a carcinogen is in accordance with previous experiments demonstrating that Hras128 rats are more sensitive to a 7,12-dimethylbenz[*a*]anthracene (DMBA) or 4NQO in the mammary or tongue tumors than were wild-type SD rats (11,21). In addition, Miyamoto *et al* demonstrated that the rasH2 mouse carcinogenesis model is highly susceptible to 4NQO induced tongue and esophageal tumors (12). In the present study, after three weeks of 4NQO treatment DH of the tongue epithelium in Hras128 rats markedly increased with respect to incidence and number, when compared with this lesion in SD rats (Fig. 3). The incidence and number of tongue tumors (PAP and SCC) also markedly increased after 6 weeks of 4NQO exposure, and this increase persisted until the end of the experiment (at experimental-week 14), when compared with these lesions in SD rats. In conventional 4NQO initiated carcinogenesis models, oral tumors are induced during 22-32 experimental weeks (11,22). In the present model, tongue tumors can be induced in only a short period of 14 experimental weeks. We therefore conclude that 4NQO-induced tongue carcinogenesis was extensively enhanced in the Hras128 rat.

Human oral cancer is a focal disorder (3), and experimental studies have indicated that there is a multistage process in the development of the oral lesions, in which dysplasias process to SCC through PAP (11,12). The results obtained in the present study showing that Hras128 and SD rats developed DH and tumors in a time-dependent manner (Fig. 3) is consistent with the established facts on human oral cancer. In addition, because of the ease of examining the lesions, the oral cavity is an excellent target organ for experimental studies. Therefore, the DH lesion may provide a useful biomarker for clarifying detailed carcinogenesis process and also provide clues to causative agents in human oral cancer.

The Ha-*ras* codon 12 and 61 mutations in human oral SCC occur at a frequency of approximately 35% (22). Previously we have reported that mutations in the *ras* family genes are 17% in 4NQO induced rat tongue tumors (23). The current Hras128 rats carry copies of the human c-Ha-*ras* transgene in their genome (15). The alkylating agent 4NQO is a powerful carcinogen in several organs (10), and it causes Ha-*ras* gene mutations by forming DNA adducts especially to guanine (N2, N7 and N8 positions) or adenine (N1 and N6 positions) (24-26). In a parallel study using Hras128 rats (unpublished data), no mutations were found in either endogenous rat c-Ha-*ras* gene or exogenous human c-Ha-*ras* gene in any tissue of DH, PAP SCC and normal mucosa, suggesting that in the present model the oral dysplasias progress to SCC via a mechanism, not involving mutational activation of the *ras* gene. In previous experiments, the transduced exogenous human c-Ha-*ras* gene was somatically mutated in the tumors of *N*-methyl-*N*-nitrosourea induced mammary carcinogenesis and *N*-butyl-*N*-(4-hydroxybutyl)nitrosamine induced urinary bladder carcinogenesis models (13,15). In these studies, however, no mutation was found in the endogenous gene. Similar results were also seen in a human c-Ha-*ras* transgenic mouse model (12). Therefore, it is likely that mutation in the transgene itself is not necessarily crucial for malignant progression and that these unique aspects in mutation status may reflect the different susceptibilities of different organs to specific carcinogens or the specificity of gene-carcinogen interactions. However, it remains to be determined whether the *ras* protein accumulates in the cytoplasm and nucleus of these tumors.

Overexpression of cyclin D1 has been found in both human and rat oral tumors (27,28). Overexpression of COX2 has been found in human oral cancer and DMBA induced hamster cheek pouch tumor (29,30). In the present study, we found that in tumor samples of Hras128 rats treatment of 4NQO caused a marked increase in the levels of mRNA expression of cyclin D1 and COX2, when compared to the adjacent normal mucosa (Fig. 5). We also found that treatment of 4NQO resulted in a significant increase in PCNA positive index in the tumor of Hras128 rats, when compared to the normal mucosa (Fig. 4). These analyses were performed in samples obtained at 14 weeks of the experiment. Thus, these results suggest that enhanced cell proliferation cooperates with the up-regulation of cyclin D1 and COX2 to cause a rapid induction of tongue tumors. We also found that mRNA expression levels of p53 and $p21^{CIP1}$ were marginally increased in the tumor of 4NQO-treated Hras128 rats (Fig. 5). This may be consistent with the study by Seo *et al* demonstrating that up-regulation of p53 and $p21^{CIP1}$ is a possible mechanism of nucleotide excision repair in response to 4NQO induced DNA damage (31).

The 4NQO-induced Hras128 rat oral carcinogenesis model may provide a system for evaluation of the mechanisms of multistage oral carcinogenesis and detection of causative agents in human oral cancer. Using this system, we also examined whether the model can be used to identify possible cancer preventive agents. A selective COX2 inhibitor, nimesulide (4-nitro-2-phenoxymethanesulphonanilide) was tested for its modifying effects on 4NQO-induced tongue carcinogenesis. We found that treatment of Hras128 rats with nimesulide caused a significant and dose-dependent decrease in tumor incidence and multiplicity compared to the control (Table IIIA). In Hras128 rats, treatment of nimesulide markedly decreased the level of expression of COX2 mRNA in the tumor compared to the adjacent normal mucosa. Therefore, the present model may also have some relevance and application to identify cancer preventive agents for human oral cancer. In summary, 4NQO rapidly causes dysplasia in oral squamous epithelia, which leads to PAP and SCC, as it does in human oral lesions. We consider the present Hras128 rat model a simple and rapid system that can be used for assessment of oral carcinogenesis and cancer prevention.

Acknowledgements

This study was supported by a Grant-in-Aid from the Ministry of Health, Labour, and Welfare of Japan, and a Grant-in-Aid from the Ministry of Education, Culture, Sports, Science and Technology of Japan.

References

1. Parkin DM, Bray F, Ferlay J and Pisani P: Global cancer statistics, 2002. CA Cancer J Clin 55: 74-108, 2005.
2. Stewart BW and Kleihues P: World Cancer Report, WHO Press, Lyon, 2003.
3. Smith CJ: Global epidemiology and aetiology of oral cancer. Int Dent J 23: 82-93, 1973.
4. Slaughter DP, Southwick HW and Smejkal W: Field cancerization in oral stratified squamous epithelium; clinical implications of multicentric origin. Cancer 6: 963-968, 1953.
5. Patel V, Leethanakul C and Gutkind JS: New approaches to the understanding of the molecular basis of oral cancer. Crit Rev Oral Biol Med 12: 55-63, 2001.
6. Davis S and Severson RK: Increasing incidence of cancer of the tongue in the United States among young adults. Lancet 2: 910-911, 1987.
7. Greenlee RT, Hill-Harmon MB, Murray T and Thun M: Cancer statistics, 2001. CA Cancer J Clin 51: 15-36, 2001.
8. Mackenzie J, Ah-See K, Thakker N, Sloan P, Maran AG, Birch J and Macfarlane GJ: Increasing incidence of oral cancer amongst young persons: what is the aetiology? Oral Oncol 36: 387-389, 2000.
9. Tanaka T, Kohno H, Sakata K, Yamada Y, Hirose Y, Sugie S and Mori H: Modifying effects of dietary capsaicin and rotenone on 4-nitroquinoline 1-oxide-induced rat tongue carcinogenesis. Carcinogenesis 23: 1361-1367, 2002.
10. Nakahara W, Fukuoka F and Sugimura T: Carcinogenic action of 4-nitroquinoline-N-oxide. Gan 48: 129-137, 1957.
11. Suzuki R, Kohno H, Suzui M, Yoshimi N, Tsuda H, Wakabayashi K and Tanaka T: An animal model for the rapid induction of tongue neoplasms in human c-Ha-ras proto-oncogene transgenic rats by 4-nitroquinoline 1-oxide: its potential use for preclinical chemoprevention studies. Carcinogenesis 27: 619-630, 2006.
12. Miyamoto S, Yasui Y, Kim M, Sugie S, Murakami A, Ishigamori-Suzuki R and Tanaka T: A novel rasH2 mouse carcinogenesis model that is highly susceptible to 4-NQO-induced tongue and esophageal carcinogenesis is useful for preclinical chemoprevention studies. Carcinogenesis 29: 418-426, 2008.
13. Asamoto M, Ochiya T, Toriyama-Baba H, Ota T, Sekiya T, Terada M and Tsuda H: Transgenic rats carrying human c-Ha-ras proto-oncogenes are highly susceptible to N-methyl-N-nitrosourea mammary carcinogenesis. Carcinogenesis 21: 243-249, 2000.
14. Asamoto M, Toriyama-Baba H, Ohnishi T, Naito A, Ota T, Ando A, Ochiya T and Tsuda H: Transgenic rats carrying human c-Ha-ras proto-oncogene are highly susceptible to N-nitrosomethylbenzylamine induction of esophageal tumorigenesis. Jpn J Cancer Res 93: 744-751, 2002.
15. Ota T, Asamoto M, Toriyama-Baba H, Yamamoto F, Matsuoka Y, Ochiya T, Sekiya T, Terada M, Akaza H and Tsuda H: Transgenic rats carrying copies of the human c-Ha-ras proto-oncogene exhibit enhanced susceptibility to N-butyl-N-(4-hydroxybutyl)nitrosamine bladder carcinogenesis. Carcinogenesis 21: 1391-1396, 2000.